Computational Materials Science 69 (2013) 510–519

Contents lists available at SciVerse ScienceDirect

Computational Materials Science

journal homepage: www.elsevier.com/locate/commatsci

On molecular statics and surface-enhanced continuum modeling of nano-structures

D. Davydov, A. Javili, P. Steinmann *

Applied Mechanics, University of Erlangen–Nuremberg, Egerlandstr. 5, 91058 Erlangen, Germany

ARTICLE INFO

Article history:
Received 15 October 2012
Received in revised form 9 November 2012
Accepted 28 November 2012
Available online 22 January 2013

Keywords:
Atomistic to continuum
Surface elasticity
Nano-materials
Surface-enhanced continuum theory

ABSTRACT

Possible links between discrete and continuum formulations have been discussed in the scientific community since several decades. Different atomistic expressions for the continuum fields (most importantly stresses) were proposed. As an example, it is possible to link discrete models to a continuum formulation based on spatial averaging in the Eulerian configuration followed by probability (statistical) averaging. As an alternative to Eulerian averaging, Lagrangian averaging has been recently proposed. Both approaches allow calculation of the local continuum fields from atomistic simulations.

From the continuum formulation perspective, the behavior of solids at the nanoscale can be captured based on a surface-enhanced continuum (SEC) theory whereby the surface is equipped with its own constitutive structure. A distinct advantage of continuum models over their atomistic counterparts is the increased computational efficiency.

In this contribution we compare atomistic fields obtained from molecular statics (MS) simulations to their counterpart, obtained from numerical approximations to the SEC theory. Bulk elastic parameters for the continuum constitutive model are obtained directly from the atomistic model. A representative numerical simulation of face-centered-cubic (FCC) copper is used to compare the two approaches.

The ability of the continuum formulation enhanced with a surface energy to model size effects, as observed in the atomistic simulations, is shown. The local fields evaluated using both the continuum and discrete approach are in a good agreement. The dependence of the results obtained from the atomistic-to-continuum procedure on both the averaging radius and the proximity of the free surface is studied. Eulerian and Lagrangian averaging approaches are shown to give comparable results for the here considered FCC crystal.

1. Introduction

Continuum mechanics has been proven to be a reliable and efficient tool to solve many problems at different length and time scales. Modern technology, however, operates at length-scales much lower than usually considered in the continuum formulation. At that scale it is not enough to consider only bulk energy, however, surface energy becomes more and more dominant with a decrease of size. Thus, the solution to a boundary value problem is not any longer independent of the dimensions, on the contrary – pronounced size effects are observed. This can be modeled by enhancing the continuum theory with a surface energy, entropy, etc.

Phenomenological models that endow the surface with its own energy date back to the pioneering work of Gibbs [1]. More recently, Gurtin and Murdoch [2] described surface effects using tensorial surface stresses (see also [3,4] for the case of thermomechanical interfaces). Daher and Maugin [5] invoked the method of virtual power to endow the surface or interface with its own thermodynamic constituents. The continuum approach of this work takes as its point of departure the surface elasticity formulation detailed by Javili and Steinmann [6]. The validation of such SEC models as compared to atomistic simulations shall be carried out.

With the continuing increase in computational power, nano-scale problems can be solved with (discrete) atomistic models such as MS. In MS a finite number of (infinitesimal) particles usually endowed only with translational degrees of freedom are considered. The primary input to such models is the interparticle potential, which is often obtained from first principles calculations. Unlike in their continuum counterparts, nothing needs to be added to the atomistic model to capture surface effects. They arise naturally due to the termination of long-range interparticle forces. MS simulations, however, are computationally very demanding. Thus, a distinct advantage of continuum models over their atomistic counterparts is the increased computational efficiency.

Since both the discrete and the continuum approach can be used to model structures at the nano-scale, the question on the correspondence between the two approaches arises. In particular,

* Corresponding author. Tel.: +49 (0)9131 85 28501; fax: +49 (0)9131 85 28503.
E-mail addresses: denis.davydov@ltm.uni-erlangen.de (D. Davydov), ali.javili@ltm.uni-erlangen.de (A. Javili), paul.steinmann@ltm.uni-erlangen.de (P. Steinmann).

0927-0256/$ - see front matter © 2012 Elsevier B.V. All rights reserved.
http://dx.doi.org/10.1016/j.commatsci.2012.11.053

kinematic and kinetic continuum quantities (such as displacements, the deformation gradient, and Cauchy stress) should be expressible in terms of the MS quantities. That is important not only for the validation of the computationally efficient continuum simulations against discrete models, but also for enhancing and developing methods that couple discrete and continuum formulations. That is, in different parts of a domain different formulations can be used. In order to bridge these domains, several methods have recently been proposed. Among such methods are the Quasi-continuum method [7–10], the Bridging-domain method [11,12], the Bridging-scale-method [13], methods based on the averaging procedure used here [14,15] and others [16,17], to name a few. For an overview on coupling methods we refer to [18,19]. Park et al. [20], Park and Klein [21] developed an alternative continuum framework based on the surface Cauchy–Born model, an extension of the classical Cauchy–Born model, to include surface stresses (see also [22]).

The framework we use here to link the discrete and continuum models dates back to works of Irving and Kirkwood [23] and Noll [24]. This linkage is achieved by spatial averaging in the current (Eulerian) configuration, followed by statistical (probability density) averaging. In the last few decades many publications were devoted to this field, see among others [25–30] and references therein. It was shown in [31], that the integral of the Cauchy stress obtained by this type of averaging over space is consistent with the Virial pressure, which is commonly used as a macroscopic measure of stress in discrete systems, thus indirectly proving the validity of the Eulerian averaging approach. As an alternative to the averaging in the current (Eulerian) configuration, it was recently proposed to average instead in the reference (Lagrangian) configuration [32]. The link between the two averaging methods is not trivial, the validity of the Lagrangian approach was numerically illustrated [32] only for the case of homogeneous solutions.

In this contribution we focus on two different averaging approaches – Eulerian and Lagrangian. The kinematic and kinetic local fields evaluated from the MS simulations are compared to the results of calculations based on a SEC formulation. Note that Yvonnet et al. [33] have recently studied the applicability of the SEC formulation in modeling Wurtzite structured nano-wires by fitting data from ab initio calculations (see also [34]).

The paper is organized as follows: In Section 2 we briefly introduce the notation adopted here and review the theoretical background for a SEC formulation as well as the link between the continuum and discrete formulation of MS. In Section 3 we study different numerical examples on FCC-type copper crystal. First, we discuss a procedure to obtain the bulk elastic properties from the molecular statics simulations. Then, both Lagrangian and Eulerian averaging procedures are benchmarked in two simple homogeneous solution cases. Finally, we study an example with a non-homogeneous solution and compare the results obtained by the discrete and continuum formulation. By changing the dimensions of the problem, the size effect is highlighted and studied. The discussion and conclusions are presented in Section 4.

2. Theory

The purpose of this preliminary section is to summarize certain key concepts in continuum mechanics and atomistic modeling, as well as to introduce the notation adopted here. Detailed expositions on non-linear continuum mechanics can be found in Truesdell and Noll [35], Marsden and Hughes [36], among others.

2.1. Notation and definitions

Direct notation is adopted throughout. Occasional use is made of index notation, the summation convention for repeated indices being implied. The N-dimensional Euclidean space is denoted $\mathbb{E}^N$. The scalar product of two vectors $\boldsymbol{a}$ and $\boldsymbol{b}$ is denoted $\boldsymbol{a}\cdot\boldsymbol{b}=[\boldsymbol{a}]_i[\boldsymbol{b}]_i$. The scalar product of two second-order tensors $\boldsymbol{A}$ and $\boldsymbol{B}$ is denoted $\boldsymbol{A}:\boldsymbol{B}=[\boldsymbol{A}]_{ij}[\boldsymbol{B}]_{ij}$. The composition of two second-order tensors $\boldsymbol{A}$ and $\boldsymbol{B}$, denoted $\boldsymbol{A}\cdot\boldsymbol{B}$, is a second-order tensor with components $[\boldsymbol{A}\cdot\boldsymbol{B}]_{ij}=[\boldsymbol{A}]_{im}[\boldsymbol{B}]_{mj}$. The action of a second-order tensor $\boldsymbol{A}$ on a vector $\boldsymbol{a}$ is given by $[\boldsymbol{A}\cdot\boldsymbol{a}]_i=[\boldsymbol{A}]_{ij}[\boldsymbol{a}]_j$. The tensor product of two vectors $\boldsymbol{a}$ and $\boldsymbol{b}$ is a second-order tensor $\boldsymbol{D}=\boldsymbol{a}\otimes\boldsymbol{b}$ with $[\boldsymbol{D}]_{ij}=[\boldsymbol{a}]_i[\boldsymbol{b}]_j$. Gradients of a quantity $\{\bullet\}$ with respect to the material and spatial configuration are denoted, respectively, as $\nabla_X\{\bullet\}$ and $\nabla_x\{\bullet\}$. Let $\boldsymbol{I}$ and $\boldsymbol{i}$ denote the identity tensors in the material and spatial configurations, respectively. Divergence operators with respect to the material and spatial configurations, respectively denoted as Div and div, are defined by

$$\mathrm{Div}\{\bullet\}:=\nabla_X\{\bullet\}:\boldsymbol{I},\qquad \mathrm{div}\{\bullet\}:=\nabla_x\{\bullet\}:\boldsymbol{i}.$$

Greek superscripts are used to define the atomistic quantities. Thus, any scalar g or vector $\mathbf{g}$ quantity attributed to particle α is denoted as g^α or $\mathbf{g}^\alpha$, respectively. The total time derivative of $\mathbf{g}^\alpha$ is denoted $\mathbf{g}^\alpha_\tau$ and the partial time derivative is denoted $\mathbf{g}^\alpha_t$. The norm of a vector $\boldsymbol{g}$ is denoted $|\boldsymbol{g}|=\sqrt{\boldsymbol{g}\cdot\boldsymbol{g}}$.

2.2. Atomistic to continuum

Molecular dynamics simulations deal with systems containing a huge number of particles N. Such particles are often considered to have translational degrees of freedom only. Thus, the state of the system is fully described by the following phase-space coordinates

$$\mathbf{z}=\{\mathbf{x}=\{\mathbf{x}^\alpha\},\mathbf{p}=\{\mathbf{p}^\alpha\}\}\in\mathbb{E}^{3N}\times\mathbb{E}^{3N} \tag{1}$$

where $\mathbf{x}^\alpha$ is the position and $\mathbf{p}^\alpha$ is the linear momentum of particle α.

The motion of the system follows the second Newton law

$$\mathbf{p}^\alpha_\tau=\mathbf{f}^\alpha \tag{2}$$

where $\mathbf{f}^\alpha$ is the total force acting on particle α and $_{;\tau}$ denotes total time derivative.

In what follows, we consider no external forces and only conservative interparticle forces, i.e.

$$\mathbf{f}^\alpha=-\nabla_{\mathbf{x}^\alpha}U(\{\mathrm{x}^{\beta\gamma}\}) \tag{3}$$

where U is the total potential energy of the system, which depends on all the interparticle distances $\mathrm{x}^{\beta\gamma}=|\mathbf{x}^{\beta\gamma}|=|\mathbf{x}^\beta-\mathbf{x}^\gamma|$.

In the MS simulations the system is considered at zero temperature ($T=0$). Thus, particle positions $\mathbf{x}$ are obtained by

$$\min_{\mathbf{x}}U\rightarrow\nabla_{\mathbf{x}^\alpha}U=\mathbf{0} \tag{4}$$

minimizing the total potential energy U.

In order to link the particle system to a continuum formulation we follow the approach originally proposed in [23,24]. Let us define a ς-distribution (space-distribution) of an (extensive) property g attributed to each particle α at spatial position $\boldsymbol{x}$ as

$$\overset{\varsigma}{\mathrm{g}}(\mathbf{z},\boldsymbol{x})=\sum_\alpha\overset{\varsigma}{\mathrm{g}}{}^\alpha(\mathbf{z},\boldsymbol{x}):=\sum_\alpha\mathrm{g}^\alpha(\mathbf{z})w(\mathbf{x}^\alpha-\boldsymbol{x}) \tag{5}$$

where $w(\boldsymbol{y})$ is the space averaging kernel which satisfies the normalization conditions

$$\int_{\mathcal{S}}w(\mathbf{x}^\alpha-\boldsymbol{x})\,\mathrm{d}\boldsymbol{x}=1 \tag{6}$$

in the vector space of translations $\mathcal{S}$.

As an example, the mass density at the spatial position $\boldsymbol{x}$ can be calculated based on the mass of each particle as

$$\varrho(\boldsymbol{x}):=\sum_\alpha\mathrm{m}^\alpha w(\mathbf{x}^\alpha-\boldsymbol{x}) \tag{7}$$

Together with statistical averaging in terms of the probability density of the system this approach can be used to obtain the continuum balance equations and expressions for the corresponding fluxes. In the MS case considered here, the expression for the (microscopic) Cauchy stress results in [37,31]:

$$\boldsymbol{\sigma}(\boldsymbol{x}) = -\frac{1}{2}\sum_{\alpha\beta}\mathbf{f}^{\alpha\beta}\otimes\mathbf{x}^{\alpha\beta}\int_0^1 w\,(\mathbf{x}^{\alpha}-\boldsymbol{x}-\alpha\mathbf{x}^{\alpha\beta})\,\mathrm{d}\alpha \tag{8}$$

where $\mathbf{f}^{\alpha\beta}$ is the force acting on particle α from particle β. From Euler's second law it follows [37] that $\mathbf{f}^{\alpha\beta}\sim\mathbf{x}^{\alpha\beta}$, thus $\boldsymbol{\sigma}(\boldsymbol{x})$ is symmetric for any interatomic potential.

In [31] we proved, that for any averaging kernel w in the case of MS the following result holds

$$\int_{\mathcal{S}}\boldsymbol{\sigma}(\boldsymbol{x})\,\mathrm{d}\boldsymbol{x} = -\frac{1}{2}\sum_{\alpha\beta}\mathbf{f}^{\alpha\beta}\otimes\mathbf{x}^{\alpha\beta}. \tag{9}$$

Thus, the macroscopic stress of the particle system equals the commonly used Virial stress, which reads in the MS case

$$\boldsymbol{\Sigma}^{\text{virial}} = -\frac{1}{2V}\sum_{\alpha\beta}\mathbf{f}^{\alpha\beta}\otimes\mathbf{x}^{\alpha\beta} \tag{10}$$

Note, that the averaging in the above is performed in the current (Eulerian) configuration. In a similar manner one can apply the same approach based on the reference (Lagrangian) configuration [32]. This leads to the corresponding expression for the Piola stress

$$\boldsymbol{P}(\boldsymbol{X}) = -\frac{1}{2}\sum_{\alpha\beta}\mathbf{f}^{\alpha\beta}\otimes\mathbf{X}^{\alpha\beta}\int_0^1 w\,(\mathbf{X}^{\alpha}-\boldsymbol{X}-\alpha\mathbf{X}^{\alpha\beta})\,\mathrm{d}\alpha \tag{11}$$

where $\mathbf{X}^{\alpha}$ is the position of particle α in the reference (Lagrangian) configuration. Moreover, the displacement $\boldsymbol{u}(\boldsymbol{X})$ and the deformation gradient $\boldsymbol{F}(\boldsymbol{X})$ have explicit expressions in the Lagrangian averaging approach:

$$\boldsymbol{u}(\boldsymbol{X},\tau) = \frac{\sum_\alpha \mathrm{m}^\alpha \mathbf{u}^\alpha w(\mathbf{X}^\alpha-\boldsymbol{X})}{\sum_\alpha \mathrm{m}^\alpha w(\mathbf{X}^\alpha-\boldsymbol{X})} \tag{12}$$

$$\boldsymbol{F} = \boldsymbol{I} + \frac{\sum_\alpha \mathrm{m}^\alpha[\mathbf{u}^\alpha-\boldsymbol{u}(\boldsymbol{X})]\otimes\nabla_X w(\mathbf{X}^\alpha-\boldsymbol{X})}{\sum_\alpha \mathrm{m}^\alpha w(\mathbf{X}^\alpha-\boldsymbol{X})} \tag{13}$$

where $\mathbf{u}^\alpha := \mathbf{x}^\alpha - \mathbf{X}^\alpha$ is the displacement of particle α. Thus, once the atomistic Piola stress and the deformation gradient are evaluated in the Lagrangian averaging approach, the corresponding value for the Cauchy stress is trivially obtained. The latter can be compared to the value of the atomistic Cauchy stress calculated from the Eulerian averaging in Eq. (8).

2.3. Surface-enhanced continuum (SEC) theory

Consider a continuum body that is deformed from the material configuration $\mathcal{B}_0$ at time $t = 0$ to the spatial configuration $\mathcal{B}_t$ at a later time $t > 0$ as shown in Fig. 1. The placements $\boldsymbol{x}$ and $\boldsymbol{X}$ in the spatial and the material configurations, respectively, are related by the invertible (non-linear) deformation map $\boldsymbol{x} = \boldsymbol{\varphi}(\boldsymbol{X})$. The outward unit normals to the boundaries $\mathcal{S}_0 = \partial\mathcal{B}_0$ and $\mathcal{S}_t = \partial\mathcal{B}_t$ are denoted $\hat{\mathrm{N}}$ and $\hat{\mathrm{n}}$, respectively. The associated deformation gradient (invertible linear tangent map) $\boldsymbol{F}$ between the material and spatial line elements, denoted $\mathrm{d}\boldsymbol{x}\in T\mathcal{B}_t$ (tangent space to $\mathcal{B}_t$) and $\mathrm{d}\boldsymbol{X}\in T\mathcal{B}_0$ (tangent space to $\mathcal{B}_0$) respectively is defined by

$$\mathbf{F} = \nabla_X\boldsymbol{\varphi}(\boldsymbol{X},t).$$

The surface of the continuum body is described (covered) by a two-dimensional manifold in the three-dimensional embedding Euclidean space. The placements of material points on the surface, denoted $\hat{\boldsymbol{x}}$ and $\hat{\boldsymbol{X}}$ in the spatial and material configurations respectively, are related by the invertible (non-linear) deformation map $\hat{\boldsymbol{x}} = \boldsymbol{\varphi}(\hat{\boldsymbol{X}}) := \hat{\boldsymbol{\varphi}}(\hat{\boldsymbol{X}})$. The surface deformation gradient $\hat{\mathrm{F}}$ (i.e. the non-invertible linear surface tangent map) between line elements $\mathrm{d}\hat{\boldsymbol{X}}\in T\mathcal{S}_0$ and $\mathrm{d}\hat{\boldsymbol{x}}\in T\mathcal{S}_t$ is defined by

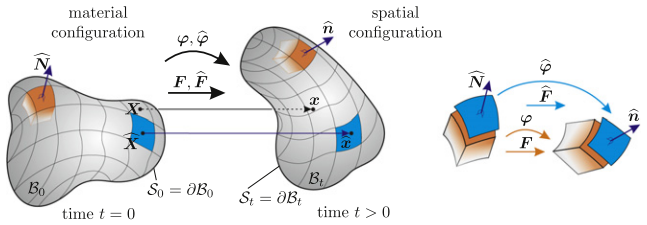

Fig. 1. The material and spatial configurations of a continuum body. The deformation gradient $\boldsymbol{F}$ and the surface deformation gradient $\hat{\mathbf{F}}$ map line elements in the bulk, and on the surface, respectively.

$$\hat{\mathbf{F}} := \widehat{\nabla_X}\,\hat{\boldsymbol{\varphi}}(\hat{\boldsymbol{X}}). \tag{14}$$

The surface gradient and divergence operators in the material configuration are respectively defined by

$$\widehat{\nabla_X}\{\bullet\} := \nabla_X\{\bullet\}\cdot\hat{\boldsymbol{I}} \quad\text{and}\quad \widehat{\mathrm{Div}}\{\bullet\} := \widehat{\nabla_X}\{\bullet\} : \hat{\boldsymbol{I}},$$

where $\hat{\boldsymbol{I}} := \boldsymbol{I} - \hat{\boldsymbol{N}}\otimes\hat{\boldsymbol{N}}$ denotes the mixed-variant surface unit tensor in the material configuration.

Remark 1. The assumption that the surface is "fixed" to the enclosed continuum via kinematic slavery is made, that is

$$\hat{\boldsymbol{x}} = \boldsymbol{x}|_{\mathcal{S}_t}. \qquad \square$$

The balance of linear and angular momentum for continua with surface structure is stated here without proof. A detailed derivation is given in [6]. The governing equations, expressed in terms of referential quantities, read

$$\begin{aligned} &\mathrm{Div}\,\boldsymbol{P}+\boldsymbol{f}=\boldsymbol{0} \quad\text{and}\quad \boldsymbol{F}\cdot\boldsymbol{P}^{\mathrm{t}} = \boldsymbol{P}\cdot\boldsymbol{F}^{\mathrm{t}} \quad \forall\boldsymbol{X}\in\mathcal{B}_0,\\ &\widehat{\mathrm{Div}}\,\hat{\boldsymbol{P}}+\hat{\boldsymbol{f}}^{\mathrm{p}}-\boldsymbol{P}\cdot\hat{\boldsymbol{N}}=\boldsymbol{0} \quad\text{and}\quad \hat{\boldsymbol{F}}\cdot\hat{\boldsymbol{P}}^{\mathrm{t}} = \hat{\boldsymbol{P}}\cdot\hat{\boldsymbol{F}}^{\mathrm{t}} \quad \forall\hat{\boldsymbol{X}}\in\mathcal{S}_0. \end{aligned} \tag{15}$$

The bulk *Piola* stress tensor is denoted $\boldsymbol{P}$ while $\hat{\boldsymbol{P}}$ is the surface *Piola* stress tensor possessing the superficiality property

$$\hat{\boldsymbol{P}}\cdot\hat{\boldsymbol{N}} = \boldsymbol{0}.$$

The body force field per unit reference volume of the bulk is denoted as $\boldsymbol{f}$. The surface force field per unit reference area of the surface consists of the (prescribed) external traction field exerted on the surface $\hat{\boldsymbol{f}}^{\mathrm{p}}$ and the traction field due to the coupling with the bulk $\boldsymbol{P}\cdot\hat{\boldsymbol{N}}$. Note that the term $\widehat{\mathrm{Div}}\,\hat{\boldsymbol{P}}$ in Eq. (15) is *not necessarily* tangent to the surface. Furthermore, the first-order tensors $\hat{\boldsymbol{f}}^{\mathrm{p}}$ and $\boldsymbol{P}\cdot\hat{\boldsymbol{N}}$ have components both tangent and normal to the surface.

For the assumption of a St. Venant elastic material the Piola stress in the bulk is calculated via the relation

$$\boldsymbol{P} = \frac{1}{2}\boldsymbol{F}\cdot[\mathbb{C} : [\boldsymbol{F}^{\mathrm{t}}\cdot\boldsymbol{F}-\boldsymbol{I}]], \tag{16}$$

in which $\mathbb{C}$ denotes the fourth-order constitutive tensor associated with cubic anisotropic materials. The surface Piola stress, which follows from an isotropic surface free energy, reads

$$\hat{\boldsymbol{P}} = \left[\hat{\lambda}\ln\hat{J}-\hat{\mu}\right]\hat{\boldsymbol{F}}^{-\mathrm{t}}+\hat{\mu}\hat{\boldsymbol{F}}+\hat{\gamma}\hat{J}\,\hat{\boldsymbol{F}}^{-\mathrm{t}} \quad\text{with}\quad \hat{J} = \widehat{\mathrm{Det}}\hat{\mathbf{F}}, \tag{17}$$

where $\hat{\gamma}$ denotes the surface tension and $\hat{\mu}$ and $\hat{\lambda}$ are solid-like (elastic) surface material parameters. Note that for a two-dimensional setting both parameters $\hat{\mu}$ and $\hat{\lambda}$ act in the same fashion and therefore $\hat{\lambda}$ is assumed to vanish for simplicity. Here it is not crucial to accurately determine the surface material parameters for the most general case.[1]

[1] In fact, the assumption of surface isotropy is not applicable in general. Nevertheless, the numerical example, when comparing atomistic and finite element results, is designed such that this assumption is valid.

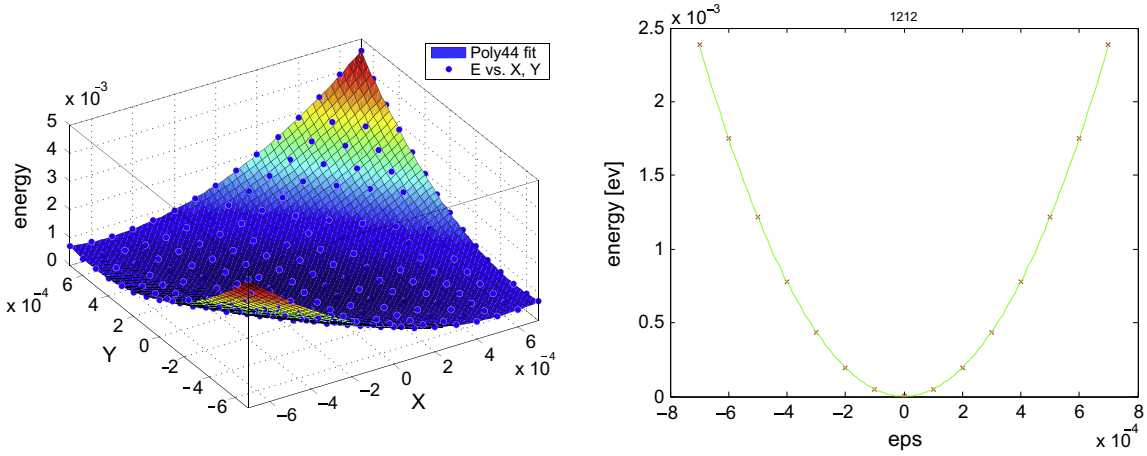

Fig. 2. Polynomial fit of the total energy for different deformation gradients. Left: energy landscape for tension in X and Y directions; Right: energy of the system in shear.

The objective of this manuscript is rather to show that the SEC theory is capable of representing the material behavior observed from atomistic simulations if a proper parameter identification process is carried out. The finite element computations are substantially more efficient than their atomistic counterparts and can be applied to a variety of situations in contrast to the atomistic calculations that are usually limited to, e.g. small sizes and low temperatures. For the details of the finite element implementation of the SEC theory see Javili and Steinmann [38,39] or Yvonnet et al. [40] based on the XFEM approach for the case of small-strain (see also [41] for an extension of the XFEM approach using a more general definition of the interface (surface)).

3. Numerical examples

In what follows we consider a FCC crystal of copper. On the atomistic side it is modeled using the EAM potential by Foiles et al. [42], which has the lattice parameter $a = 3.615$ A at zero temperature and the cut-off radius 4.94 A. Atomistic simulations are performed using the LAMMPS open-source software [43]. The quartic averaging kernel of radius R was used to evaluate the continuum fields from the atomistic simulations:

$$w(r) = \frac{35}{8\,V}\,[1 - r^2]^2 \tag{18}$$

with $r = |\mathbf{x}^\alpha - \boldsymbol{x}|/R$ and $V = \frac{4}{3}\pi R^3$.

Since the total potential energy U is readily available from the atomistic simulation, the bulk linear elastic parameters can be obtained by evaluation of the second order derivate of the energy with respect to the applied deformation:

$$C_{ijkl} = \frac{1}{V}\frac{\partial^2 U}{\partial \epsilon_{ij}\epsilon_{kl}} \tag{19}$$

From this procedure the cubic anisotropy continuum parameters are obtained as (in GPa): $C_{11} = 167.26$, $C_{12} = 124.15$, $C_{44} = 76.44$. Here second-order derivatives are calculated using polynomials fitted to the atomistic potential energy (Fig. 2). Periodic boundary conditions are considered for the here studied representative volume element (RVE) for both the atomistic and continuum descriptions.

3.1. Homogeneous deformation

This section serves as a benchmark to evaluate the here used approaches of calculating the local (microscopic) continuum quantities from the atomistic simulations.

3.1.1. Bulk

Consider a RVE (Fig. 3) with periodic boundary conditions under uniaxial loading, i.e.

$$\mathbf{F} = \begin{bmatrix} F_{11} & 0 \\ 0 & 1 \end{bmatrix} \tag{20}$$

The averaging radius $R = 2.3 \cdot a$ was chosen. On the atomistic side, the macroscopic deformation gradient $\boldsymbol{F}$ is produced through an affine displacement of all atoms. No additional energy minimization step is needed for the case of homogeneous deformation of a simple crystal.

The results of a uniaxial deformation of the homogeneous RVE are presented in Figs. 3 and 4. It is clear, that the atomistic system behaves in a non-linear elastic way. Thus, the linear continuum description based on the fitted parameters for Eq. (19) compares well to the atomistic one only in the range of small deformations, approximately below 1%. Both Lagrangian and Eulerian approaches to link the atomistic simulations to the continuum description result in almost the same Cauchy stress values, which also equal the macroscopic stress (Virial). Thus, the validity of the averaging approaches is proven, at least for the homogeneous solution case.

3.1.2. Variation in space

Next, the dependence of the continuum fields obtained from the atomistic simulations on the radius of the averaging kernel as well as the presence of boundaries is studied. To this end, a simulation domain as shown on Fig. 5 is considered. Periodic boundary conditions are considered in x and y directions while in z direction the slab has a finite thickness of 10 unit cells. The uniaxial deformation gradient is produced through an affine displacement of all atoms. Our goal here is not to study surface effects, but rather the averaging approach in the proximity of boundaries.

Fig. 6 shows the resulting stresses plotted from the center of the RVE towards the free surface. The dotted horizontal lines indicate the continuum analytical solution as if there is no free surface. It is clear, that the results of the averaging procedure are questionable when evaluated close to the free-surface. That is not surprising considering the fact, that the boundary or the volume of the discrete system in general cannot be uniquely defined. Essentially, the averaging procedure smears out the boundary.

For the averaging radius employed here ($2.3 \cdot a$), the obtained results are artefact-free when evaluated further than 2.5 unit cells from the boundary. This estimate will be important when we will discuss results of the next numerical example.

Note, that when the averaging radius is too small, there are fluctuations of the calculated continuum quantities in the bulk of the

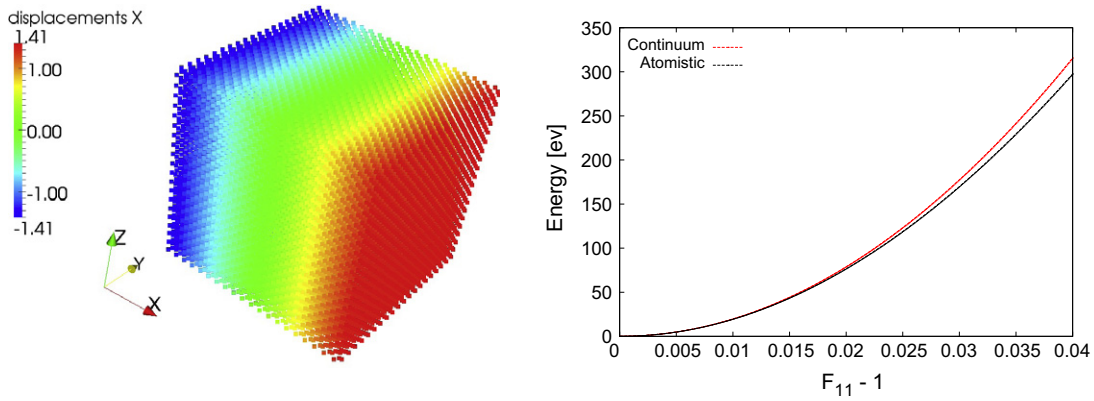

Fig. 3. Left: Atomistic displacements in x direction in a homogeneous periodic RVE for a 4% uniaxial stretch. Right: The total energy E comparison during uniaxial stretching of bulk FCC crystal as evaluated from atomistic simulations and continuum solution.

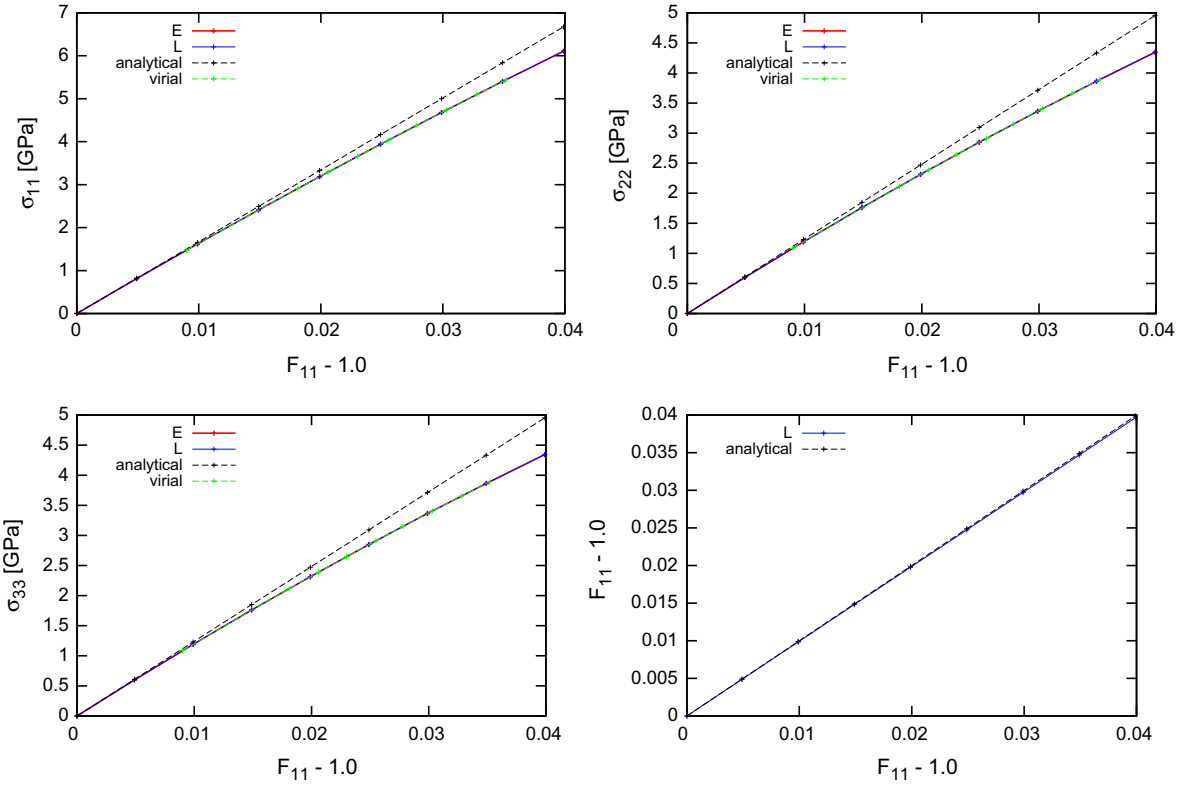

Fig. 4. Cauchy stress evaluated in the center of the RVE from the atomistic simulations. Eulerian and Lagrangian stress measures are compared to the continuum solution and the macroscopic Virial stress.

crystal. Otherwise, the evaluated fields agree very well with the continuum solution.

3.2. Non-homogeneous deformation

A uniaxial tension of the RVE which consists of a 2d plate with a hole (Fig. 7) is considered. We aim to compare the atomistic simulations to the continuum using both the integral and local quantities.

From the atomistic simulation point of view, a square plate oriented along the crystallographic axes is considered as a RVE. The number of unit cells in the third dimension was fixed to three, ranging in the other two dimension from 40 to 200. In all numerical examples the ratio between the diameter of the hole and the width of the plate is kept equal 1/5. Crystal lattice atoms positions are considered as the reference configuration.

Loading is applied in two stages.

1. All atoms within the cylinder of a given radius are removed from the perfect lattice configuration. Due to the missing neighbors, the system is not in equilibrium any longer. Thus, the total energy can be minimized which results in the displacement of atoms. On the continuum side, that corresponds to the loading due to the introduction of the surface energy.
2. The macroscopic deformation gradient $\boldsymbol{F}$ is applied to the atomistic configuration obtained previously using the following procedure:

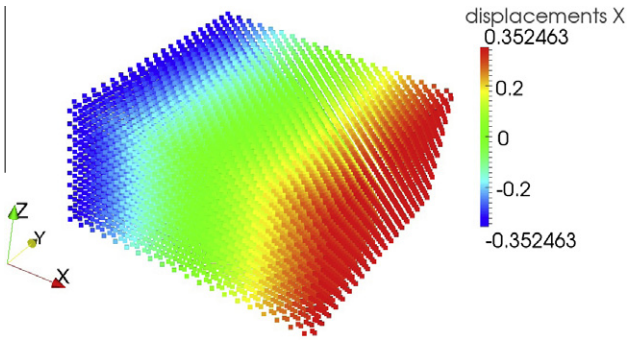

Fig. 5. Atomistic displacements in the slab under uniaxial tension produced through an affine displacement of atoms. Periodic boundary conditions are considered in x and y directions whereas in z direction a finite thickness of 10 unit cells is considered. Top and bottom boundaries of the slab correspond to the [100] crystallographic surface.

- First, the dimensions of the RVE are changed according to the prescribed uniaxial deformation gradient $\boldsymbol{F}$, followed by a corresponding homogeneous affine displacement of all particles in the domain, i.e. particles positions $\mathbf{x}$ are remapped to the new domain.
- Second, keeping the RVE dimensions fixed, the total energy of the system is minimized with respect to particles positions.

The size effect is observed by varying the total length of the plate while keeping its ratio to the hole radius constant. Fig. 8 depicts the atomistic and continuum homogenized stresses corresponding to the different lengths at the relaxed and loaded configurations. For the atomistic solution it is evaluated via Eq. (10), whereas for the continuum model it is the sum of the integral of the bulk stresses over the bulk and the integral of the surface stresses over the surface and the whole divided by the volume of the RVE (see [44] for more details about the energetically consistent definitions of overall stress of the RVE).

In general, we can conclude that the size effect is well captured both qualitatively and quantitatively by the continuum formula-

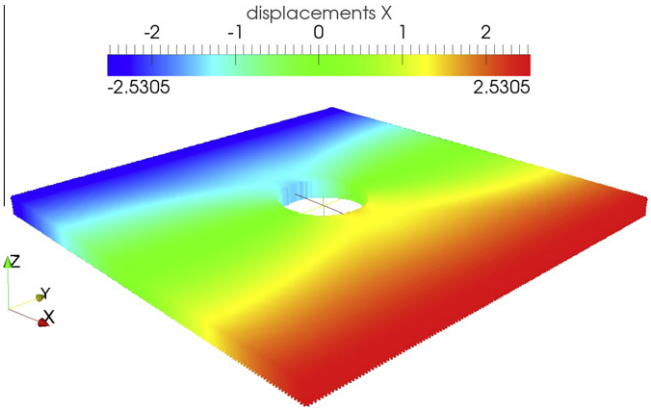

Fig. 7. Atomistic displacements in x direction in the plate with a hole under the uniaxial deformation gradient of 1%. Periodic boundary conditions are considered in all directions.

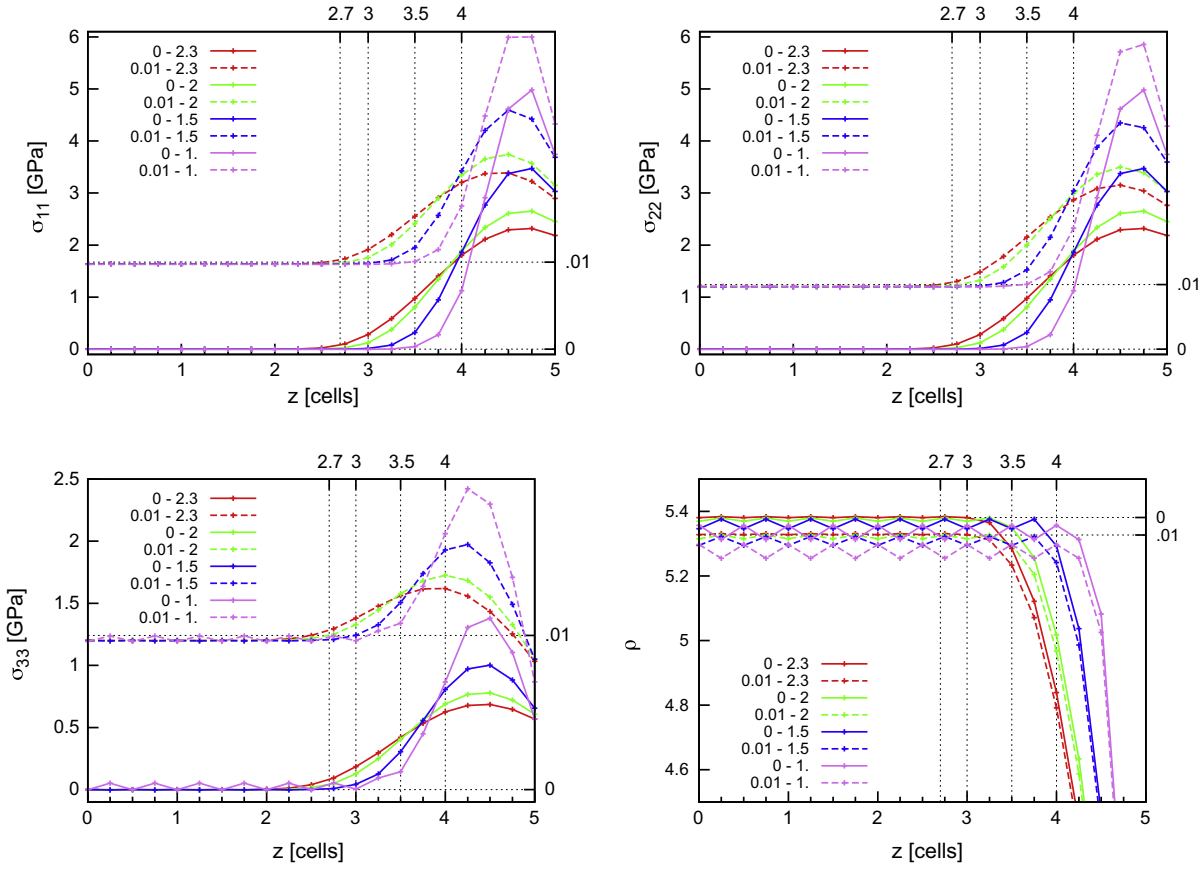

Fig. 6. Stress and density profiles along the height of the slab as obtained from the Eulerian averaging procedure with different radius of the spatial kernel evaluated at the initial and 1% loaded configuration. The first number in the legend denotes the amount of uniaxial strain, whereas the second – the radius of averaging. Horizontal lines indicate analytical continuum solution.

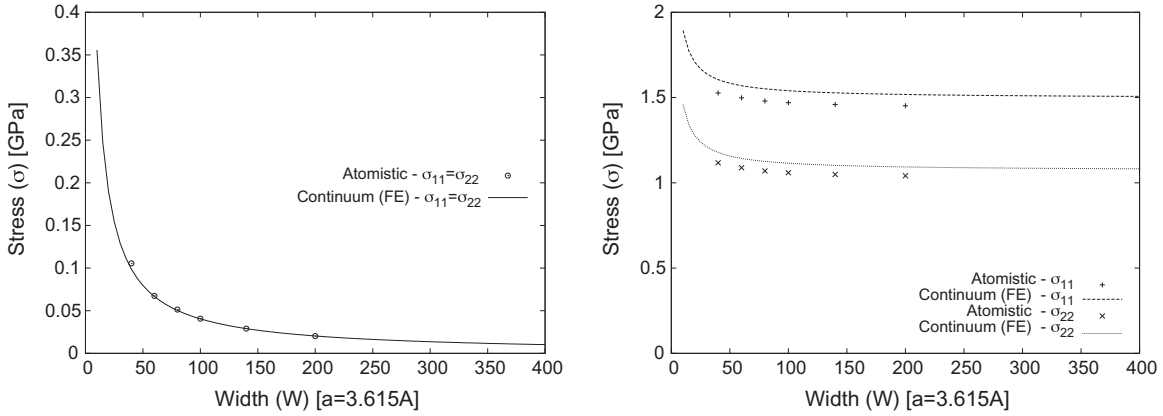

Fig. 8. Atomistic and continuum homogenized stresses corresponding to the different lengths at the relaxed (left) and 1% uniaxially loaded (right) configurations of the plate with a hole. The geometry is fixed while width of the RVE varies.

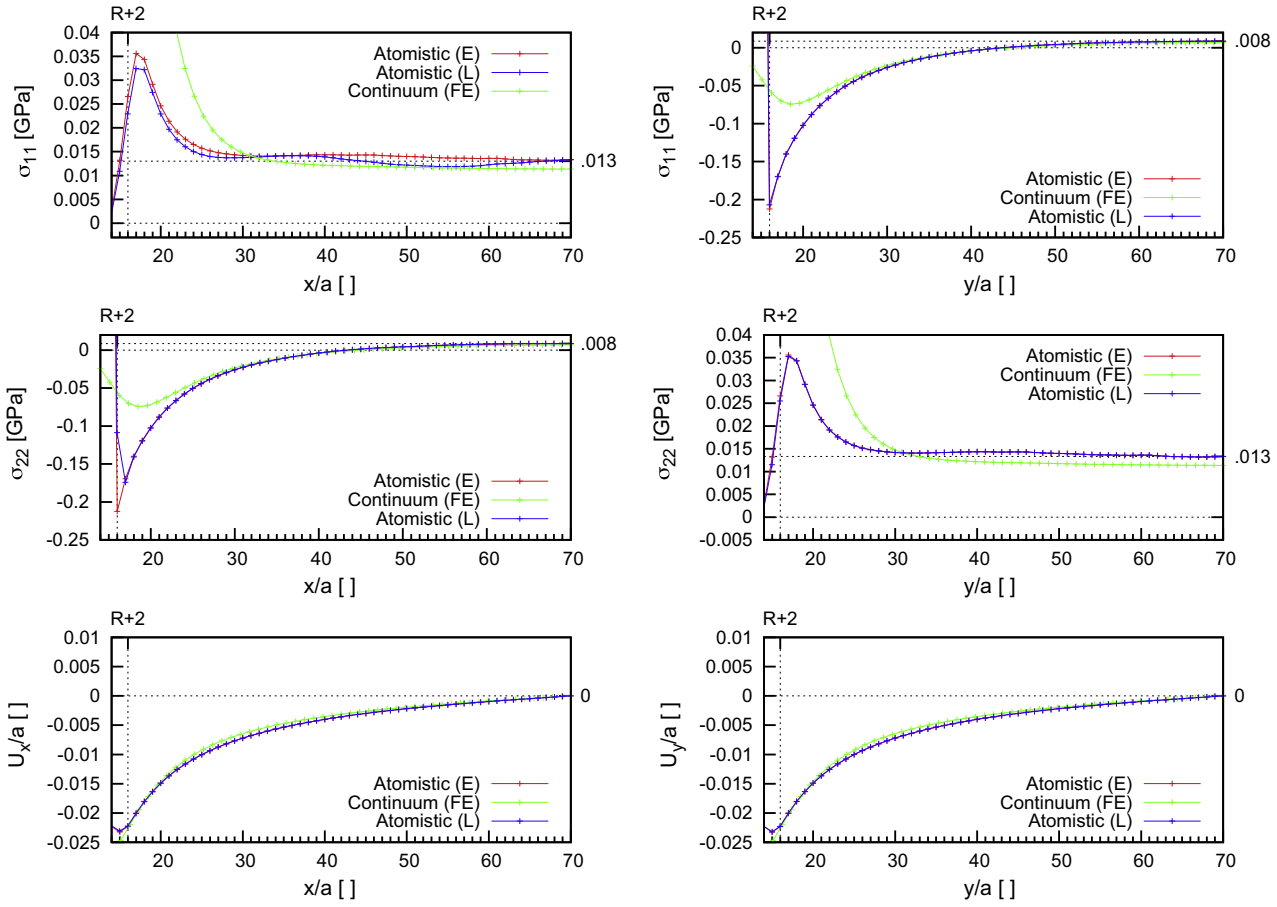

Fig. 9. Microscopic stresses and displacements in the plate with a hole due to surface tension only (no-stretch) as evaluated from continuum solution and Eulerian and Lagrangian averaging procedure of atomistic simulations.

tion. Note, that even though the considered surface is not isotropic from the atomistic point of view, the isotropic continuum description shows a good agreement to capture the macroscopic size effect for the toy problem here. The discrepancy for the uniaxially-loaded case is less than 5% and is most likely due to the intrinsically non-linear elastic behavior of the FCC crystal (see Fig. 4).

Next, the local Cauchy stresses and displacements from the atomistic and continuum approaches are compared. The results below are calculated for the plate of the width of 140 unit cells, evaluated along the $x = 0$ and $y = 0$ lines. The stress and displacements profiles for the relaxed and loaded configuration are presented on Figs. 9 and 10, respectively. On the continuum side, the two unknown surface parameters were obtained by a trial-and-error procedure of fitting the atomistic results.

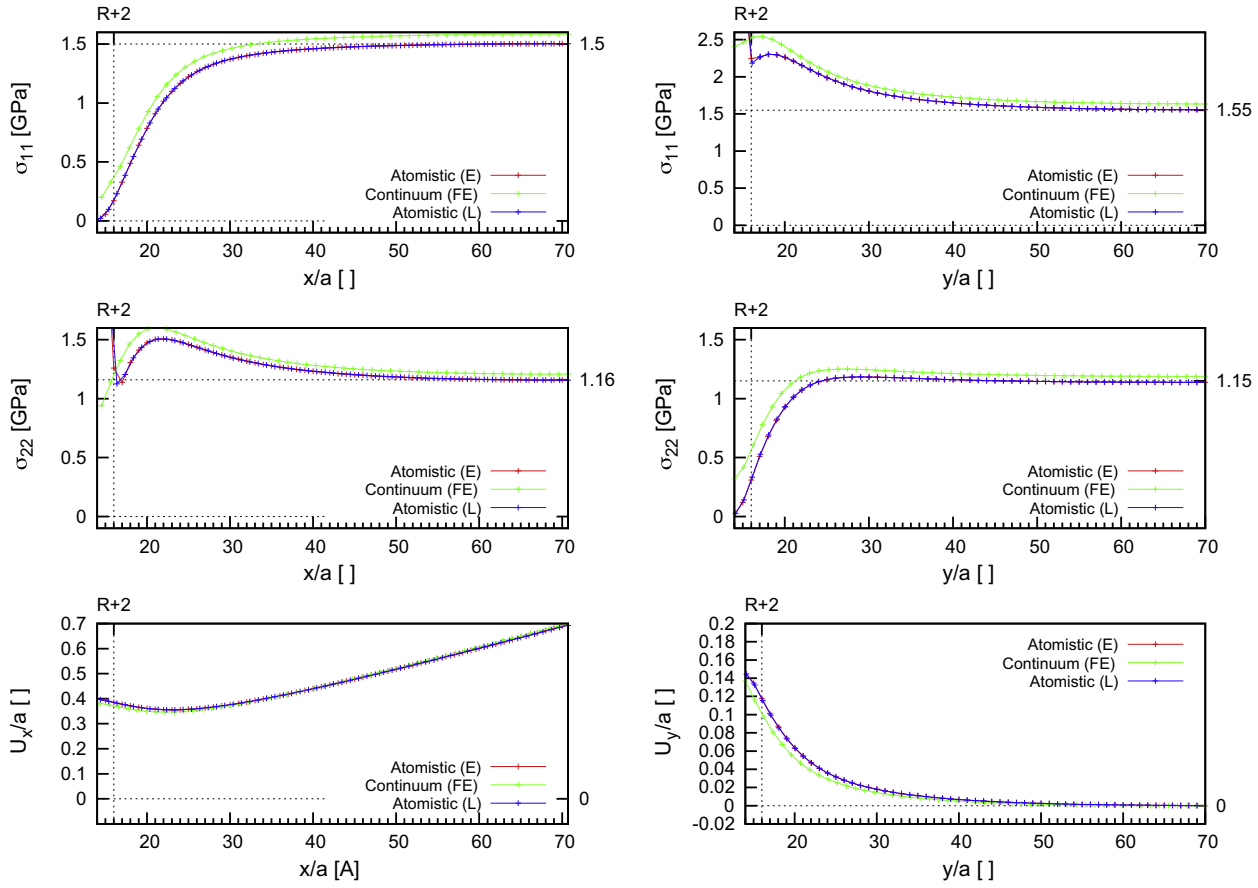

Fig. 10. Microscopic stresses and displacements in plate with a hole for uniaxial deformation of 1%. Eulerian and Lagrangian averaging procedures of atomistic simulations are compared to SEC solution. The discrepancy for the uniaxially-loaded case is most likely due to the intrinsically non-linear elastic behavior of the bulk FCC crystal.

Both a quantitatively and qualitatively good agreement between the discrete and continuum models is observed.

The small fluctuations in terms of stresses in Fig. 9 can probably be explained by unsufficient applicability of the method for small perturbations from the equilibrium state, as noted in [45] where the authors observed less fluctuation for the loaded case as compared with the stress evaluated in the relaxed state. Indeed, observe that there is no non-physical fluctuations for the 1% loaded case.

Note, that in the absence of the surface energy in the continuum formulation, the solution of the uniaxial loading is self-similar. That is not the case when the continuum surface energy is considered.

The full picture of the stress and displacement distribution in the uniaxially deformed RVE as well as the relaxed one under only surface tension calculated from the continuum formulation is presented in Fig. 11. Also, the evolution of stresses and displacements during uniaxial deformation is shown in Fig. 12.

4. Discussion and conclusions

In this contribution we compared the continuum mechanics approach enhanced with a surface energy to atomistic (MS) simulations. Lagrangian and Eulerian approaches for particle averaging were applied to the numerical examples of a FCC crystal. The size effect observed in the macroscopic stresses as evaluated from the MS simulations was well captured by the SEC formulation.

By investigating the MS simulation of the homogeneous RVE, the non-linearity of the stress–strain relationships in the FCC crystal is observed. Thus, the continuum description corresponds to the atomistic one only for relatively small deformations.[2] The microscopic (local) stresses evaluated using the Eulerian and Lagrangian approach were shown to be equal for the homogeneous deformation. Moreover, they were also equal to the Virial stress.

The results obtained from the atomistic-to-continuum procedure are dependent on both the averaging radius and the proximity of the free surface. A too small averaging radius leads to spatial fluctuations of the corresponding continuum fields even for examples with homogeneous solution. When such fields are evaluated close to free surfaces, averaging artefacts occur. That points to the fundamental difference between the continuum and discrete models: the volume which corresponds to the discrete system generally cannot be uniquely defined. The same holds for the boundary of the system. Despite the averaging boundary artefacts, the microscopic (local) atomistic fields evaluated at a distance from the free surface are in a perfect agreement with the continuum solution. That is the case for both simple (homogeneous) and non-homogeneous solutions. Thus, the correspondence between the continuum and the atomistic approaches is shown.

Eulerian and Lagrangian approaches to the atomistic averaging were compared. For a FCC crystal comparable results are observed for the two approaches. Furthermore, it is observed that the finite element results based on the SEC theory are in a good agreement

[2] Note, that the large strain formulation has been used on the continuum side.

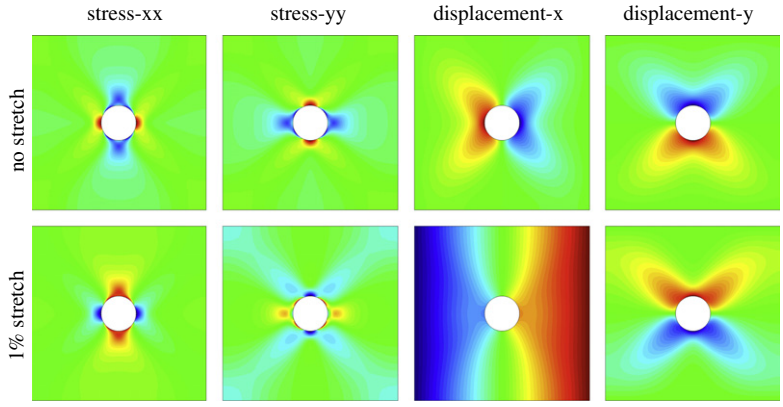

Fig. 11. Stress and displacement for no-stretch and 1% uniaxial deformation calculated by the finite element method. Corresponding values could be seen at Fig. 12.

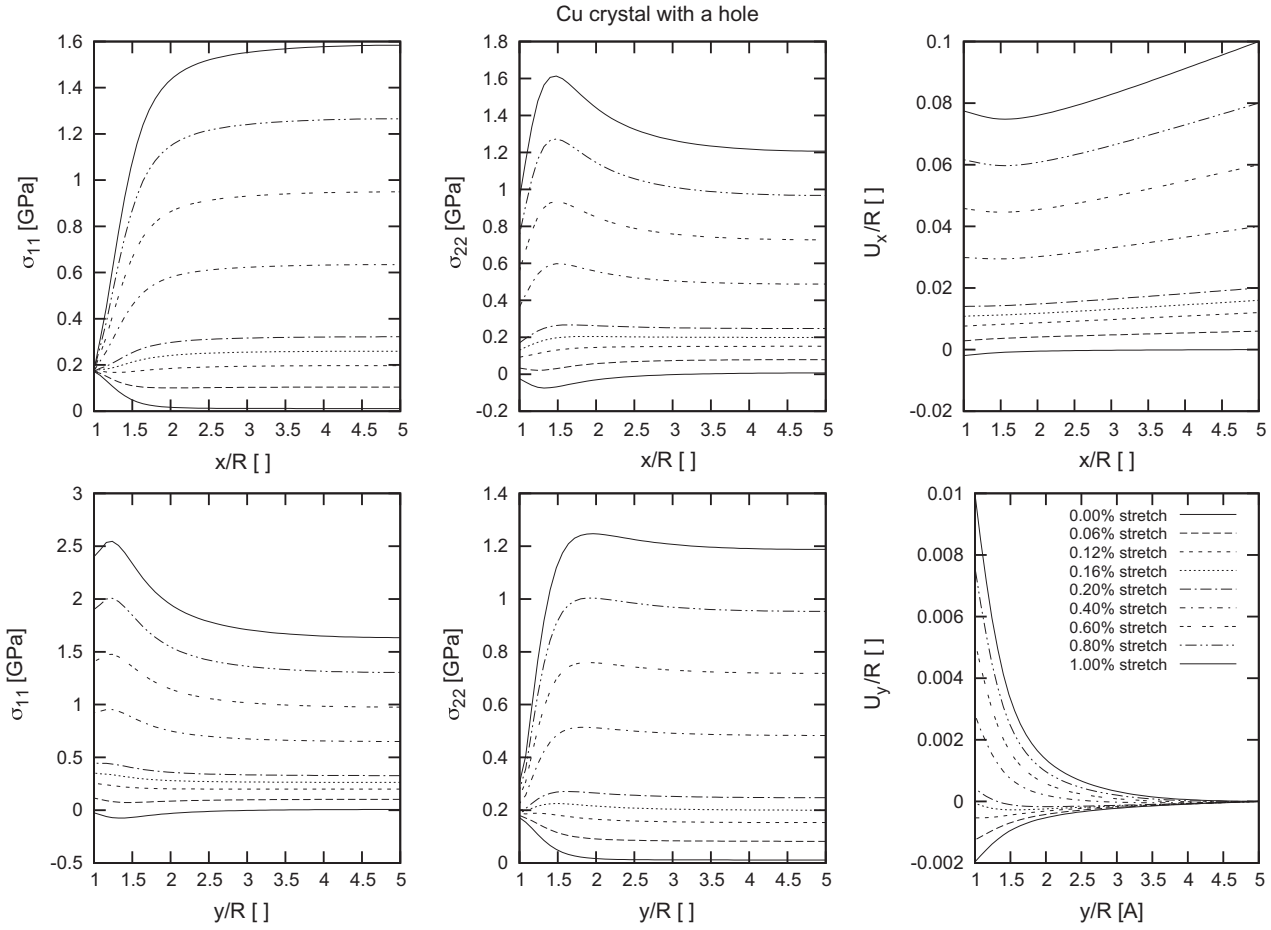

Fig. 12. The evolution of stresses and displacements during uniaxial deformation calculated by the finite element method.

with the atomistic computations. However, that observation should not be considered as a general rule. A study for more complex materials with internal deformation modes (such as polymers) is the aim of our further work.

Acknowledgments

The first author is grateful to the German Science Foundation (Deutsche Forschungs–Gemeinschaft, DFG), Grant STE 544/46-1, for the financial support. The support of this work by the ERC Advanced Grant MOCOPOLY is gratefully acknowledged by the second and third authors.

References

[1] J.W. Gibbs, The Scientific Papers of JW Gibbs, vol. 1, DoverPublications, 1961.
[2] M.E. Gurtin, A.I. Murdoch, Archive for Rational Mechanics and Analysis 57 (4) (1975) 291–323.
[3] G.P. Moeckel, Archive for Rational Mechanics and Analysis 57 (1975) 255–280.

[4] F. dell'Isola, A. Romano, International Journal of Engineering Science 25 (11–12) (1987) 1459–1468.
[5] N. Daher, G.A. Maugin, Acta Mechanica 60 (3–4) (1986) 217–240.
[6] A. Javili, P. Steinmann, International Journal of Solids and Structures 47 (24) (2010) 3245–3253.
[7] E.B. Tadmor, M. Ortiz, R. Phillips, Philosophical Magazine A: Physics of Condensed Matter, Structure, Defects and Mechanical Properties 73 (6) (1996) 1529–1563.
[8] J. Knap, M. Ortiz, Journal of the Mechanics and Physics of Solids 49 (9) (2001) 1899–1923.
[9] V. Shenoy, R. Miller, E. Tadmor, R. Phillips, M. Ortiz, Physical Review Letters 80 (4) (1998) 742–745.
[10] B. Eidel, A. Stukowski, Journal of the Mechanics and Physics of Solids 57 (1) (2009) 87–108.
[11] M. Xu, R. Gracie, T. Belytschko, International Journal for Numerical Methods in Engineering 81 (13) (2010) 1635–1658.
[12] S.P. Xiao, T. Belytschko, Computer Methods in Applied Mechanics and Engineering 193 (17–20) (2004) 1645–1669.
[13] W.K. Liu, D. Qian, S. Gonella, S. Li, W. Chen, S. Chirputkar, International Journal for Numerical Methods in Engineering 83 (8–9) (2010) 1039–1080.
[14] X. Wang, J.D. Lee, CMES – Computer Modeling in Engineering and Sciences 62 (2) (2010) 150–170.
[15] X. Zeng, X. Wang, J.D. Lee, Y. Lei, Computational Mechanics 47 (2) (2011) 205–216.
[16] P.A. Klein, J.A. Zimmerman, Journal of Computational Physics 213 (1) (2006) 86–116.
[17] X. Li, J.Z. Yang, E. Weinan, Journal of Computational Physics 229 (10) (2010) 3970–3987.
[18] W.K. Liu, E.G. Karpov, S. Zhang, H.S. Park, Computer Methods in Applied Mechanics and Engineering 193 (17–20) (2004) 1529–1578.
[19] R.E. Miller, E.B. Tadmor, A unified framework and performance benchmark of fourteen multiscale atomistic/continuum coupling methods, Modelling and Simulation in Materials Science and Engineering 17 (5) (2009).
[20] H.S. Park, P.A. Klein, G.J. Wagner, International Journal for Numerical Methods in Engineering 68 (10) (2006) 1072–1095.
[21] H.S. Park, P.A. Klein, Computer Methods in Applied Mechanics and Engineering 197 (41–42) (2008) 3249–3260.
[22] H.S. Park, P.A. Klein, Physical Review B 75 (8) (2007) 1–9.
[23] J. Irving, J.G. Kirkwood, The Journal of Chemical Physics 18 (6) (1950) 817–829.
[24] W. Noll, Journal of Rational Mechanics and Analysis 4 (1955) 627–646.
[25] N.C. Admal, E.B. Tadmor, Journal of Elasticity 100 (2010) 63–143.
[26] Y. Chen, Local stress and heat flux in atomistic systems involving three-body forces, Journal of Chemical Physics 124 (5) (2006).
[27] R. Hardy, Journal of Chemical Physics 76 (1982) 622–628.
[28] A.I. Murdoch, Journal of Elasticity 88 (2007) 113–140.
[29] M. Pitteri, Archive for Rational Mechanics and Analysis 111 (2) (1990) 99–120.
[30] R. Xu, B. Liu, Acta Mechanica Solida Sinica 22 (6) (2009) 644–649.
[31] D. Davydov, P. Steinmann, Reviewing the roots of continuum formulations in molecular systems. Part III: Stresses, Couple Stresses, Heat Fluxes, Mathematics and Mechanics of Solids, in preparation.
[32] J.A. Zimmerman, R.E. Jones, J.A. Templeton, Journal of Computational Physics 229 (2010) 2364–2389.
[33] J. Yvonnet, A. Mitrushchenkov, G. Chambaud, Q.-C. He, Computer Methods in Applied Mechanics and Engineering 200 (5-8) (2011) 614–625.
[34] A. Mitrushchenkov, G. Chambaud, J. Yvonnet, Q. He, Towards an elastic model of wurtzite AlN nanowires, Nanotechnology 21 (25) (2010).
[35] C. Truesdell, W. Noll, The non-linear field theories of mechanics, third ed., vol. 282, Springer-verlag, Berlin Heidelberg, 2004.
[36] J.E. Marsden, T.J.R. Hughes, Mathematical Foundations of Elasticity, Dover Publications, 1994. ISBN 0486678652.
[37] D. Davydov, P. Steinmann, Reviewing the roots of continuum formulations in molecular systems. Part I: Particle dynamics, statistical physics, mass and linear momentum balance equations, Mathematics and Mechanics of Solids. http://dx.doi.org/10.1177/1081286512467790.
[38] A. Javili, P. Steinmann, Computer Methods in Applied Mechanics and Engineering 198 (27–29) (2009) 2198–2208.
[39] A. Javili, P. Steinmann, Computer Methods in Applied Mechanics and Engineering 199 (9–12) (2010) 755–765.
[40] J. Yvonnet, H.L. Quang, Q.-C. He, Computational Materials Science 42 (1) (2008) 119–131.
[41] M. Farsad, F.J. Vernerey, H.S. Park, International Journal for Numerical Methods in Engineering 84 (12) (2010) 1466–1489.
[42] S.M. Foiles, M.I. Baskes, M.S. Daw, Physical Review B 33 (12) (1986) 7983–7991.
[43] S. Plimpton, Journal of Computational Physics 117 (1) (1995) 1–19. URL http://lammps.sandia.gov.
[44] A. Javili, A. McBride, P. Steinmann, J. Mergheim, U. Schmidt, Micro-to-macro transitions for continua with surface structure at the microscale, submitted for publication.
[45] J.A. Zimmerman, E.B. Webb III, J.J. Hoyt, R.E. Jones, P.A. Klein, D.J. Bammann, Modelling and Simulation in Materials Science and Engineering 12 (4) (2004) S319–S332.